Near-resonance light scattering from a high-density ultracold atomic ^{87}Rb gas

S. Balik, A. L. Win, and M. D. Havey*
Department of Physics, Old Dominion University, Norfolk, Virginia 23529, USA

I. M. Sokolov and D. V. Kupriyanov
Department of Theoretical Physics, State Polytechnic University, 195251, St. Petersburg, Russia
(Received 14 February 2013; published 13 May 2013)

We report a combined experimental and theoretical investigation of near-resonance light scattering from a high-density and ultracold atomic ^{87}Rb gas. The atomic sample, having a peak density $\sim 5 \times 10^{13}$ atoms/cm^3, temperature ~ 65 μK, and initially prepared in the $F = 1$ lower-energy ^{87}Rb hyperfine component, is optically pumped to the higher-energy $F = 2$ hyperfine level. Measurements are made of the transient hyperfine pumping process and of the time evolution of scattering of near-resonance probe radiation on the $F = 2 \rightarrow F' = 3$ transition. Features of the density, detuning, and temporal dependence of the signals are attributed to the high density and consequent large optical depth of the samples.

DOI: 10.1103/PhysRevA.87.053817 PACS number(s): 42.25.Dd, 42.50.Nn, 72.15.Rn

I. INTRODUCTION

The development of techniques to cool and trap atomic gases [1,2] has revolutionized many traditional atomic-physics research areas and, at the same time, has stimulated new connections and types of interdisciplinary specialization. In atomic physics, the original efforts were primarily directed towards observation and research on Bose-Einstein condensation [3–5]. In turn, this has stimulated a vast amount of research in a wide range of areas including quantum information science [6,7], quantum optics [8–11], precision measurements [12–14], plasma physics [15,16], and molecular spectroscopy [17,18]. These areas, and others, have been transformed by the combination of ultracold experimental facilities and theoretical understanding of the physical processes. Among the important characteristics of the utilized atomic gases are the gas temperature, density, and spin polarization. For example, storage of individual photon wave packets in ultracold gases combines quantum optical techniques of coherent dark-state formation and electromagnetically induced transparency to address a critical area of quantum information processing [19,20]. The lifetime of the atomic spin wave, which determines the storage time of the photonic information in the form of a dark-state polariton, depends on the gas temperature, collision rates, and local magnetic environment. In another research area, photoassociative formation of ultracold diatomic molecules depends quadratically on the density of the parent ultracold atomic gas. Likewise, by initiating formation of an ultracold plasma in a high-density atomic gas, one can attain strong coupling with sufficient ionization of the gas.

Over the past decade, a number of research groups [21–27] have concentrated on near-resonance light scattering in ultracold atomic gases. A particular interest has been coherent multiple scattering of light when the influence of atomic motion is of minimal importance. Then the natural length scale for the photon multiple scattering is the optical mean free path, given by $l = 1/\rho\sigma$, where ρ is the atomic density and σ the cross section for atomic light scattering in a weak field. For light of wave-vector magnitude $k = 2\pi/\lambda$, a useful dimensionless parameter is the product kl [28]. When $kl \gg 1$, the so-called weak-localization regime [23], light scattering can be thought of as a sequence of scattering and propagation events [24]. In this regime, an observable that survives configuration averaging is the coherent backscattering cone, which is a few-milliradian-width feature that displays an enhancement of as much as a factor of 2 over the incoherent albedo for backscattered light [29–31]. In ultracold atomic gases, the angular shape and peak enhancement of this spectral feature have been studied for a wide range of conditions, including spectral detuning from resonance, light polarization, probe light intensity [32], sample size and optical density, and external magnetic field [33–41]. Observation of the coherent backscattering cone established that weak-field multiple light scattering, even for resonance radiation, is a coherent process. When the atomic density is significantly increased, so that the parameter $kl \sim 1$ (the so-called Ioffe-Regel condition [28]), there are a number of atoms within a volume $1/k^3$, and light scattering [42] becomes a cooperative process [23,43–50]. In this regime, it is expected that a number of fascinating quantum optical processes, including Anderson localization of light [51–55], and atom-based random lasing [56–60], may emerge. It is these processes, and the conditions under which they might be experimentally studied that are the main motivations for the current research program.

In the present paper, we describe our experimental approach to obtaining atomic conditions, and particularly atomic densities, in the regime where $kl \sim 1$. We also describe the method we use to prepare the atomic sample so that large orders of multiple scattering may be obtained, along with the associated experimental observations and their interpretation. This is followed by presentation and discussion of experimental results of the density and detuning dependence of time-dependent light scattering on the nearly closed $F = 2 \rightarrow F' = 3$ hyperfine component of the ^{87}Rb D_2 transition. The experimental results are also compared with those obtained by rigorous theoretical treatment [43,61] of the dynamics under conditions similar to those realized in the experiments.

*mhavey@odu.edu

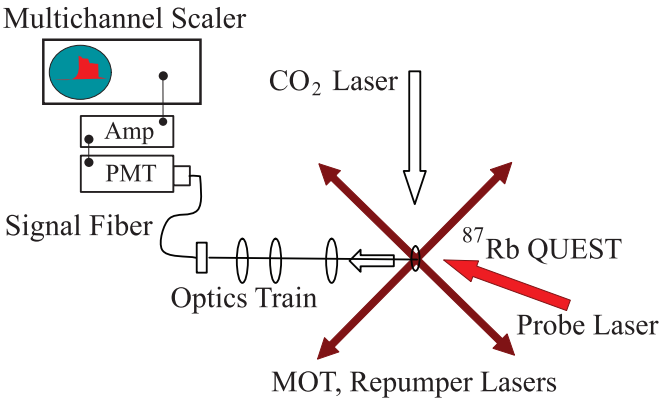

FIG. 1. (Color online) Schematic drawing of the experimental apparatus. In the figure QUEST stands for quasielectrostatic trap and PMT refers to a photomultiplier tube. MOT refers to a magneto-optical trap, while CO_2 laser indicates a carbon dioxide laser. Drawing not to scale.

II. EXPERIMENTAL APPROACH

A schematic diagram of the experimental apparatus is shown in Fig. 1, and the main optical excitation transitions used in the present experiments are shown in Fig. 2. In Fig. 1, the main focus of the instrumentation is an optical dipole trap formed in the focal region of a carbon dioxide (CO_2) laser beam. A 40 MHz acousto-optical modulator (AOM) is used to switch and to direct approximately 50 W of the 100 W CO_2 laser output to the trapping region. The trapping beam is focused to a radial spot size of $\sim$55 μm, and an associated Rayleigh range of $z_R \sim 750$ μm. Because the operating trap wavelength of 10.6 μm is far longer than those of the Rb resonance transitions, the dipole force is closely proportional to the static dipole polarizability of atomic Rb; the trap is then referred to as a quasistatic electric dipole trap (QUEST) [2]. The trap depth is approximately 650 μK and has associated measured trap angular frequencies $\omega_z = 2\pi \times 50$ rad/s and $\omega_r = 2\pi \times 1300$ rad/s. As described in detail elsewhere [62], the QUEST is loaded with atoms that have been collected from a surrounding thermal Rb vapor and cooled in an

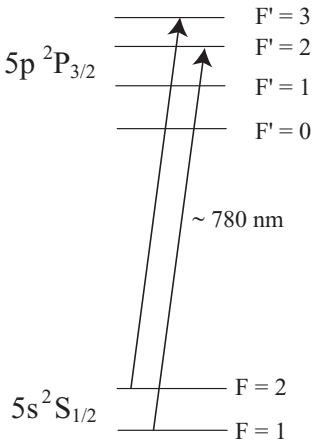

FIG. 2. Schematic energy-level diagram for ^{87}Rb showing the optical transitions important for the experiments reported in this paper. Not to scale.

overlapping magneto-optical trap (MOT). The QUEST atoms are initially loaded from the MOT into the lower-energy $F = 1$ hyperfine component of the Rb ground level. Following QUEST loading, the MOT lasers and magnetic fields are shut off, and the atoms in the dipole trap collisionally thermalize to a temperature of approximately 65 μK. After this natural thermalization process, approximately 15% of the atoms originally in the MOT have been transferred to the QUEST; this amounts to around 5×10^6 atoms. Measurements of the QUEST characteristics, after the hold period, by absorption imaging, parametric resonance, and the measured number of atoms transferred show a sample with peak density about 5×10^{13}atoms/cm^3 and a temperature of $T_o = 65$ μK. The transverse Gaussian radius is 9.6 μm, while the longitudinal radius (the Rayleigh length) is 230 μm. The $1/e$ lifetime of the confined atoms is greater than 5 s, limited by background gas collisions.

The primary goal of the experiments is to study light scattering on the nearly closed $F = 2 \rightarrow F' = 3$ hyperfine transition associated with the D_2 resonance line. However, the atoms are initially loaded into the QUEST in the $F = 1$ lower-energy hyperfine component and must be optically pumped into the higher-energy $F = 2$ level. This is accomplished by the MOT repumping laser beams, tuned resonantly to the $F = 1 \rightarrow F' = 2$ transition as indicated in Fig. 2. As described elsewhere [62] the repumper laser is an external cavity diode laser, and is locked to an ^{87}Rb saturated absorption feature associated with the $F = 1 \rightarrow F' = 2$ hyperfine transition. The laser bandwidth is approximately 0.5 MHz. The repumper delivers a beam of maximum intensity $\sim$4 mW/cm^2 and is directed along the same optical paths as the trapping laser beams. Repumper switching is controlled with an acousto-optical modulator. There are three counterpropagating pairs of such beams directed towards the sample along three orthogonal directions. The repumper intensity of $\sim$4 mW/cm^2 corresponds to an on-resonance saturation parameter larger than unity. With reference to Fig. 1, the light scattered out of the repumper beams by the atom sample is collected at an angle of 45° from the horizontal pair of repumper beams and at 90° from the vertical beam (not shown). Approximately 1% of the resulting scattered light is collected with a field lens and launched into a multimode fiber which, in turn, transports the light to an infrared-sensitive and refrigerated photomultiplier tube (PMT) operating in a single-photon-counting mode. The photon-counting pulses are amplified with a fast amplifier and then binned in a multichannel scaler with a time resolution of 5 ns. Depending on the counting rate, a data record of several thousand experimental realizations is necessary to obtain sufficient counting statistics. Each experimental realization requires several seconds for formation and interrogation of the atomic sample.

We emphasize that the hyperfine optical pumping process by which the ^{87}Rb atoms in the QUEST are brought from the $F = 1$ to the $F = 2$ ground hyperfine component is an important part of the sample preparation process. Fluorescence signals taken over a three orders of magnitude range of sample density are shown in Fig. 3. These densities, as indicated in the figure legend, represent the peak density in the central region of the atomic sample. As described previously, the sample density is reduced from its maximum value by allowing for

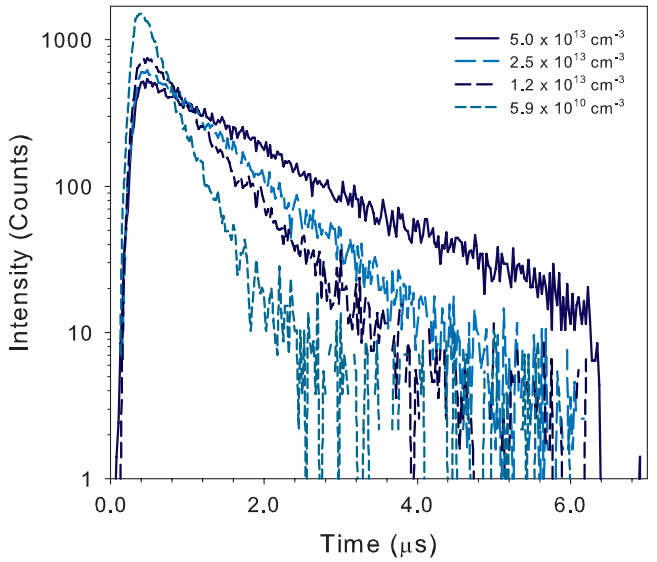

FIG. 3. (Color online) Time dependence of the light scattered during the $F = 1 \rightarrow F' = 2$ optical pumping process. From top to bottom, the curves correspond to decreasing atomic density; the values refer to the peak density at the center of the sample. The correspondence between the peak density, the transverse optical depth, and the sample dimensions can be found in Table I.

a selected period of free expansion of the sample prior to switching on the repumper laser and collecting the resulting scattered light signals. Further expansion of the sample during the data acquisition period is negligible. Several features of the data are apparent from Fig. 3. First, there is a small background signal of a few counts remaining even after the transient signals have decayed away. This behavior is more apparent in the lower-density data, which has an associated faster decay rate than the higher-density data. This signal is due to hot-atom fluorescence excited by the relatively intense repumper laser beams. Second, with the background level

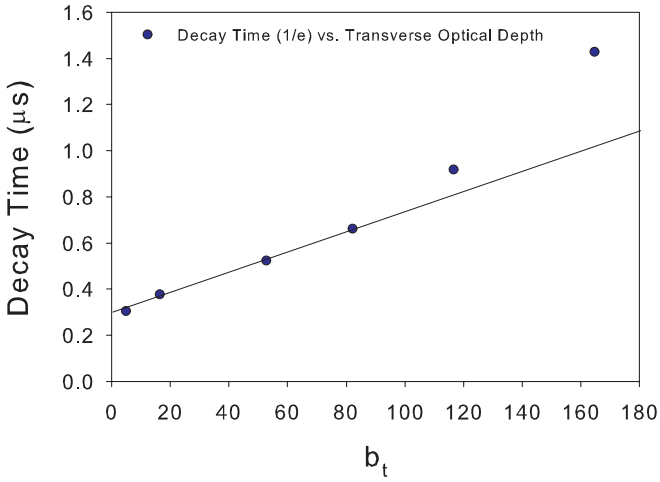

FIG. 4. (Color online) Time constant for the approximately exponential decay of the repumping fluorescence, as a function of transverse optical depth b_t, as shown in Fig. 3. The correspondence between the transverse optical depth, peak density, depth, and sample dimensions can be found in Table I.

TABLE I. QUEST parameters relating the peak transverse optical depth on the $F = 2 \rightarrow F' = 3$ transition to the peak sample density and the Gaussian radii of the atomic cloud.

Peak b_t	n_o (atoms/cm^3)	r_o (μm)	z_o (μm)
165	5.0×10^{13}	9.8	248
117	2.5×10^{13}	13.8	248
82	1.2×10^{13}	19.5	248
53	5.1×10^{12}	30.4	249
16	5.2×10^{11}	92.3	264
5	5.9×10^{10}	240	345

accounted for, the decay of the signals is well approximated by a single exponential time decay, with the higher-density data decaying at a much slower rate than the lower-density measurements display. The $1/e$ decay times for the various decay curves of Fig. 3 are presented in Fig. 4. For these data, the connection between the various values of b_t and the peak atom density can be found in Table I. The time scales associated with the optical pumping process may be crudely estimated by considering that the repumper laser beam is intense enough that it saturates the repumper transition. Then the time scale for the pumping process transferring an atom from the lower ($F = 1$) to the upper ($F = 2$) hyperfine component is approximately $2\tau_o$, where $\tau_o \sim 26$ ns is the radiative lifetime of the excited state. On the average, then, the repumper beam penetrates into the sample a distance of one optical mean free path $l = \frac{1}{\rho\sigma}$ in this time. Here ρ is the average atom density and σ is the optical scattering cross section [63] For a sample of size r_o, an estimate of the pumping time is then $\mathrm{T} \sim 2\tau_o \frac{r_o}{l}$. This simple formula provides a rough estimate of about 3 μs for the greatest optical depth of $b_t = 165$, in fair agreement with the results of Fig. 3.

We point out that in spite of the apparently simple phenomenology of the optical pumping dynamics, the physical process is in reality quite complex. For example, the atom sample is initially in the lower-energy $F = 1$ hyperfine level, and after the process is terminated, is nearly completely pumped into the $F = 2$ level. At the same time, the atom sample is initially very optically deep to the repumper laser and optically thin to the $F = 2 \rightarrow F' = 2$ inelastic Raman decay. These roles are reversed but in a spatially inhomogeneous way as the pumping dynamics take place. Beyond this, multiply scattered light on both main transitions should participate significantly in the entire dynamics (this is ignored in the estimate of the pumping time above). The entire process is made yet more complex by the inelastic components in the scattered light, these being generated by the intense repumper laser. At the greatest optical depths b_t attained in these experiments, collective effects are also very important. For these reasons, it is more useful to consider the microscopic time scale for optical pumping to be a parameter that depends on all the above processes, but that the time scale for the entire process still scales as $\frac{r_o}{l}$, which is proportional to the transverse optical depth. The data of Fig. 4 show that this expected scaling describes the data well for smaller optical depth, but for greater values, the time scale for the pumping process grows more rapidly. It is plausible that this increase is due to the influence of secondary light scattering by $F = 2 \rightarrow F' = 2$

diffusive flux in the sample; this multiply scattered light can repump the atoms back to the $F = 1$ lower hyperfine level, thus slowing the overall optical pumping process. This interpretation is consistent with the experimental observation that the total integrated scattered light intensity, although nearly constant as a function of optical depth, is measured to be somewhat larger (∼40%) at the greatest optical depth, compared to the intensity at lower b_t. Although these processes are interesting, and worthy of further study, they do not represent the primary focus of the present work. We therefore defer more quantitative theoretical modeling and and comprehensive experiments to a later study.

To close this section, in the main experimental protocol (see Fig. 1) used to obtain the results reported in the following sections, a probe beam tuned in the spectral vicinity of the $F = 2 \rightarrow F' = 3$ nearly closed transition is directed towards the sample, and the resulting scattered light signals collected by the same optical arrangement described above. The probe laser is of the same design as the repumper laser, has a bandwidth ∼3 MHz, and is switched and directed by an acousto-optical modulator towards the sample. Because of constraints on the vacuum chamber geometry, the linearly polarized probe beam is directed (see Fig. 1) at an angle of approximately 30° away from the fluorescence collection direction. The probe beam is also directed downwards at an angle of 30°. The collection and electronic accumulation of scattered light signals are the same as with the repumper signals.

Finally, we point out that in some of the experiments reported here the atomic density was varied over a wide range. This was accomplished by allowing for a period of ballistic expansion of the cloud after the QUEST was turned off. The atomic sample temperature is known, so this procedure allows the peak density or the peak optical depth to be determined. As the sample is well approximated by a two-axis Gaussian atom distribution [63], the two Gaussian radii and the peak atom density (or the total number of atoms in the sample) are sufficient to determine the two peak optical depths characterizing the sample. We summarize in Table I the peak transverse optical depth b_t, the peak atom density at the center of the sample n_o, the transverse Gaussian radius r_o, and the longitudinal Gaussian radius z_o. The optical depth refers here to that of the nearly closed $F = 2 \rightarrow F' = 3$ hyperfine transition, and is obtained by using a resonance scattering cross section of 1.36×10^{-9} cm^2. The optical depth dependence may readily be rescaled to other $F \rightarrow F'$ transitions [63].

III. RESULTS: PROBE LIGHT SCATTERING ON THE $F = 2 \rightarrow F' = 3$ TRANSITION

A. Density dependence

We first turn our attention to the broad main focus of this report, which is the situation where the hyperfine optical pumping process is completed prior to initiation of probe light scattering in the spectral vicinity of the $F = 2 \rightarrow F' = 3$ transition. In this case, the function of the hyperfine optical pumping is to transfer the atoms to the $F = 2$ ground-level hyperfine component; when this process is complete, the peak resonance optical depth on the probe transition is about 165, as indicated in Table I. We first consider the resonance response as a function of atom density under weak-field probe conditions of ∼630 μW/cm^2. For these measurements, the atom sample is exposed to a nearly rectangular temporal pulse of 2 μs duration; this pulse has a 20 dB rise and fall time of about 100 ns. The probe has a $1/e^2$ diameter of 6 mm, much larger than the dipole-trapped sample size for all conditions (see Table I). As shown in Figs. 5(a) and 5(b), the scattered light transients for all densities consist of a temporal buildup of the measured intensity to an approximate steady level, followed by a several hundred nanosecond temporal decay after the probe laser beam is extinguished. The overall time scale for each of these processes is quite similar; slight differences are due to the fact that the turn-on and turn-off temporal profiles of the probe laser intensity are similar, but not identical. We point out that the two lowest-density graphs of Fig. 5(b) have been rescaled by factors of 1.2 (for the 5.1×10^{11} atoms/cm^3 data) and 1.6 (for the 5.9×10^{10} atoms/cm^3 data). No rescaling was necessary for the other data in these graphs. This was necessary because for the lowest-density data, which corresponds to the largest sample size (see Table I), a portion of the signal expanded outside the field of view of the detection optics. This

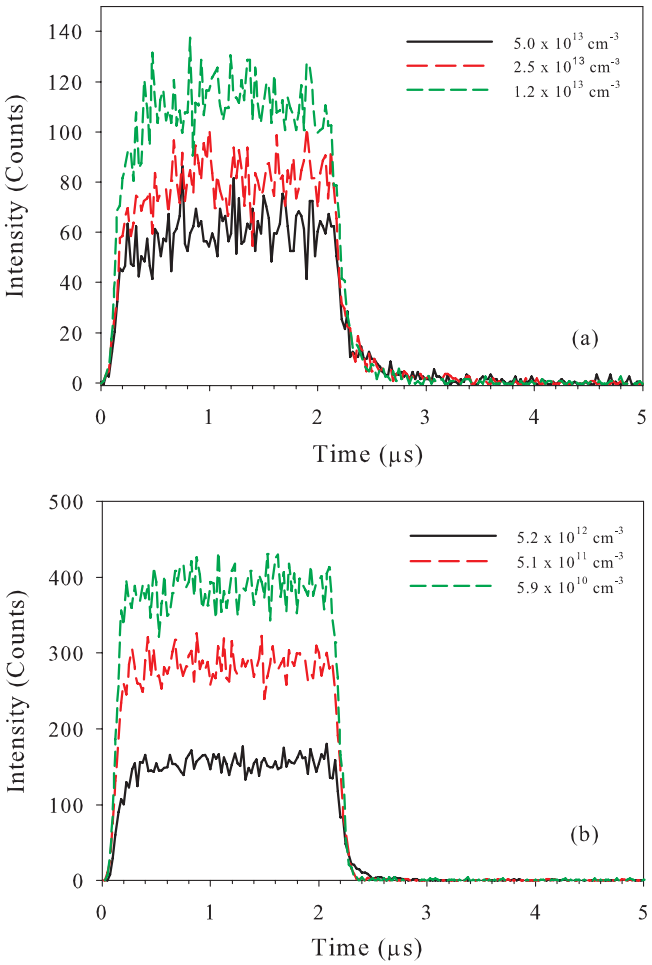

FIG. 5. (Color online) Variations of the $F = 2 \rightarrow F' = 3$ resonant probe response with density and time. Note that the maximum intensity decreases with increasing density, at constant atom number. Note also the emergence of a long-time decay after the probe excitation is shut off. (a) Dependence for (a) higher and (b) lower densities.

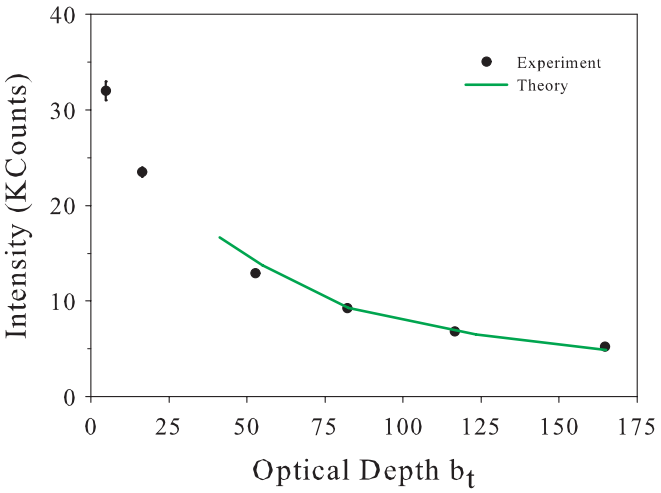

FIG. 6. (Color online) Variations of the integrated $F = 2 \rightarrow F' = 3$ resonant probe response with peak transverse optical depth. Note that the maximum intensity decreases with increasing optical depth, at constant atom number. Kcounts $= 10^3$ s^{-1}. Reproduced with permission [65].

rescaling is also made to the integrated intensity data presented in Fig. 6.

We analyze these results by considering the integrated probe signal (as in Fig. 6) as a function of decreasing atomic density. However, instead of the atomic density, we parametrize the dependence in terms of the peak transverse optical depth b_t through the center of the ellipsoidal atomic sample. The optical depth is the natural parameter to describe many characteristics of light scattering and diffusion in dense scattering media. Note that there are nominally two optical depths required to describe our atomic sample [63]. These are the peak transverse optical depth b_t, as just mentioned, and the longitudinal optical depth b_l, which is typically more than ten times larger than b_t. The variation of the integrated scattered light signals with b_t is shown in Fig. 6, where it is seen that the signals increase as the optical depth decreases. We point out that the data in Fig. 6 have been previously reported [64] and compared to theoretical results; we have provided additional experimental details here, and include the results for completeness of the present paper. The behavior evident in Fig. 6 can be physically understood from the fact that for very large b_t, only the atoms near the sample surface contribute significantly to the scattering signal. However, as the density, and correspondingly the optical depth, decreases, more of the atoms in the sample participate in the scattering, and the resulting signal increases. This behavior is a clear indicator that light scattering from these dense and cold atomic samples is a collective process.

The solid curve in Fig. 6 is a theoretical result obtained through approximate scaling laws obtained previously [64]. Those scaling relations were obtained by exploring numerically the dependence of the scattering cross sections on sample size. Such scaling rules are useful because the samples explored experimentally contain several orders of magnitude more atoms, making direct numerical simulations impractical. The details of the theoretical approach have been laid out and applied in several previous papers [43,61,64,66], and are briefly summarized in the Appendix.

B. Detuning dependence

We now turn to the detuning and time dependence of the light scattering signals. In the experiments we have measured the temporal response of the sample to a 2 μs probe pulse for detunings Δ in a ± 24 MHz range around the atomic $F = 2 \rightarrow F' = 3$ resonance. The finest temporal resolution is 5 ns, but grouping the data into larger bins of 25, 50, or 100 ns width, which we do for the results reported here, improves the signal-to-noise ratio significantly. Positive values of Δ correspond to probe frequencies larger than the isolated atom's resonance frequency.

Experimental results are compared to theoretical ones obtained for atomic samples of nearly the same peak density, but fewer atoms. The theoretical approach used has been described elsewhere [43,61,64,65,67], and for the convenience of the reader is summarized in the Appendix. To have possibilities of contrasting the results of the theory with experiments, we choose the density of our motionless four-level atoms in such a way that photons will have the same mean free path as in the ^{87}Rb samples. Estimating the resonant cross section of the light from a single atom with the $J = 0 \rightarrow J = 1$ transition as $3\lambda^2/2\pi$, we obtain that $n_0 \simeq 5 \times 10^{13}$ cm^{-3} in experiment corresponds to $n_0 \simeq 0.05k^3$ in theory.

1. Frequency-dependent time response

Representative measurements of the time response of the light scattered from the sample are given in Fig. 7, where we see that the response to the nearly rectangular probe pulse consists of a monotonic increase in signal to a nearly steady value (within the measurement statistics), followed by a decaying afterglow signal extending, in the case of excitation around bare atomic resonance, for several microseconds after the probe beam is extinguished. The time resolution of these data is 25 ns. The overall features of the results are qualitatively reasonable, for in these high-optical-depth samples, multiple scattering of light is a strong effect. Nearer atomic resonance the overall effect of multiple scattering is greater and is to slow significantly both the buildup and the decay of the sample fluorescence signals. These data are recorded under conditions of the peak transverse optical depth $b_t = 165$. The corresponding theoretical results are shown in Fig. 8, where very good qualitative agreement is seen in comparison with the measurements of Fig. 7.

2. Time-dependent spectral response: Results

We further analyze the data of Fig. 7 by extracting the response of the system at fixed times but as a function of detuning of the probe frequency from $\Delta = 0$. This procedure yields an excitation or action spectrum, and reveals how strongly probe light of a given detuning yields a response of the atomic sample. The analysis is largely done with a time resolution of 100 ns in order to obtain an improved signal-to-noise ratio in comparison with smaller bin sizes. However, for the short period during turn on of the probe pulse, we use a smaller grid of 50 ns, in order to better resolve the relatively rapid changes in the spectrum during this period. The result of that analysis for the early-time part of the turn-on spectrum is shown in Fig. 9. There we can see that the initial width is very large in comparison with

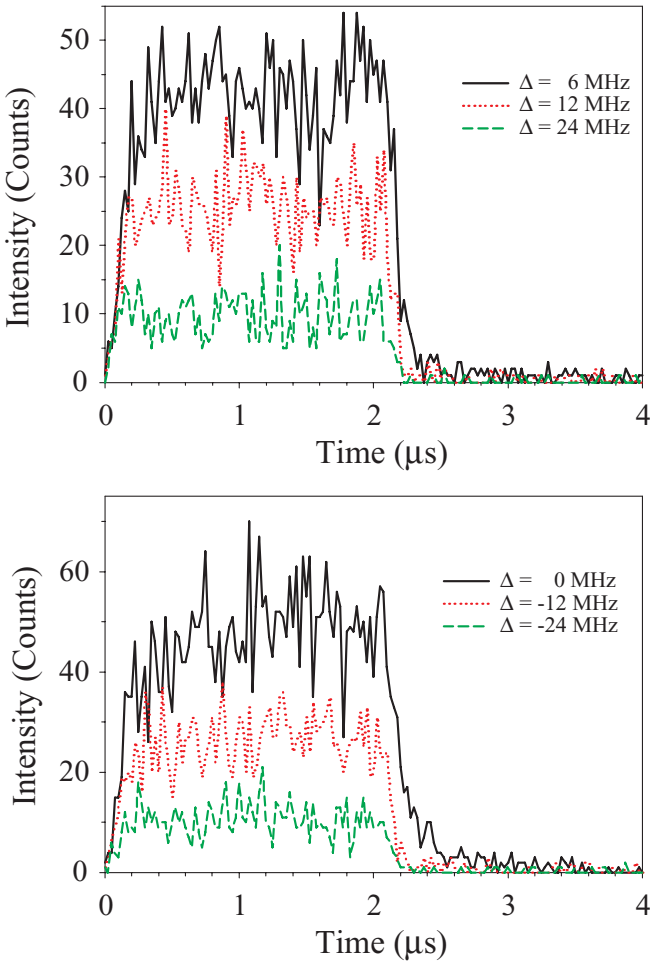

FIG. 7. (Color online) Representative spectral variations of the transient light scattering response associated with the $F = 2 \rightarrow F' = 3$ probe transition. Positive (higher-frequency) detunings are shown in (a), while negative (lower-frequency) detunings are shown in (b). These data are recorded under conditions of the peak transverse optical depth $b_t = 165$. The bin size on the time axis is 25 ns.

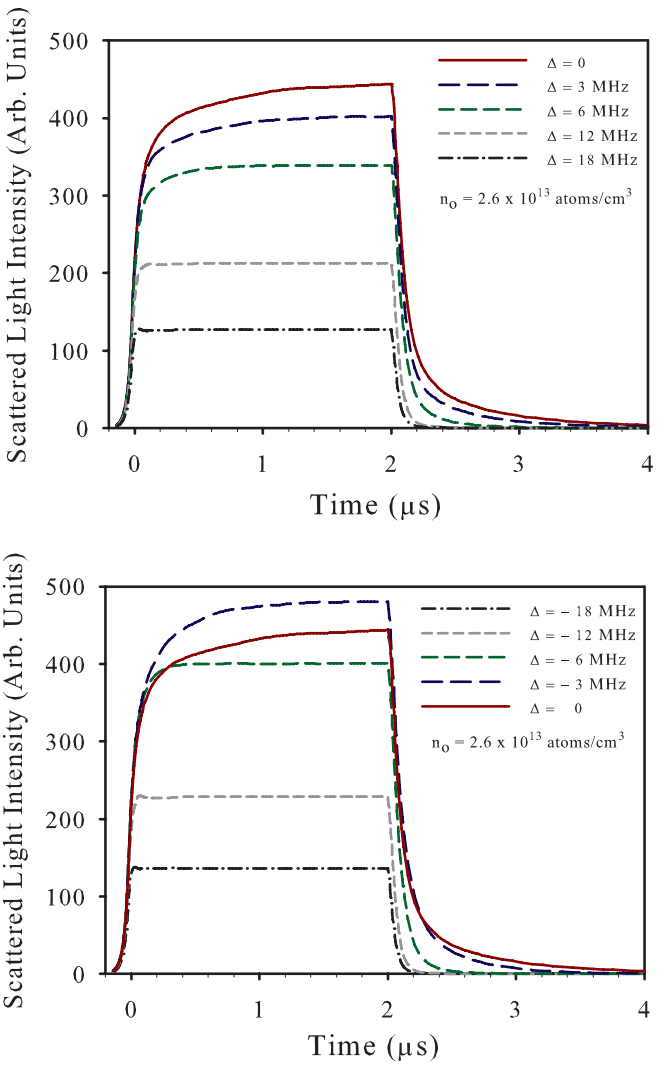

FIG. 8. (Color online) Theoretical spectral variations of the transient light scattering response associated with the $F = 2 \rightarrow F' = 3$ probe transition. Positive (higher-frequency) detunings are shown in the upper panel, while negative (lower-frequency) detunings are shown in the lower panel. The $\Delta = 0$ result is included in each graph for convenience. These results are calculated for a peak density of $n_o = 0.05$.

the approximately 6 MHz natural width of the bare-atom transition. In the figure, the solid lines through the data points represent fits of a Lorentzian line shape to the measured spectrum. This choice is not essential, although the correlation of the fit to the data is quite high. The full width of the spectral response, which is the main extracted quantity, is within a few percent for either Lorentzian or Gaussian fits. What is clear is that the spectral width of the excitation spectrum is very broad for short times and narrows quickly. A similar behavior is seen in the theoretical results presented in Fig. 10, and again, the qualitative agreement is quite good. We can broadly understand the short-time behavior by realizing that for time scales on the order of the Wigner delay time [68], the scattered light signal comes from those atoms very near the surface of the atomic cloud. If we take that thickness to extend until the optical depth $b \sim 1$, corresponding to a decrease in the probe intensity by e^{-1}, then this occurs for a detuning of the probe frequency such that $\Delta_o = \gamma/2\sqrt{b_o - 1}$, where b_o is the on-resonance transverse optical depth through the center of the cloud. For our experiment $b_o = 165$, giving a full width of $\Delta_o = \gamma\sqrt{b_o - 1} \sim 77$ MHz. This is in very good agreement with the width at very short times (see Fig. 9).

Upon turn off of the probe pulse the spectral width of the excitation spectrum decreases from a value several times the natural width to approximately 8 MHz. The experimental results illustrating this are presented in Fig. 11, while corresponding theoretical results are shown in Fig. 12. As in the spectral response upon turn on of the probe pulse, the line shape here is also well fitted by a Lorentzian form. It is important to note that the spectral width of the probe laser itself is about 3 MHz, and has a measured Gaussian power spectrum. This means that the widths determined by these measurements are slightly larger than that determined by the physical processes involved. We also note that there appears to be a small shift of the resonance response to frequencies lower than the single-atom resonance. The frequency shift of about

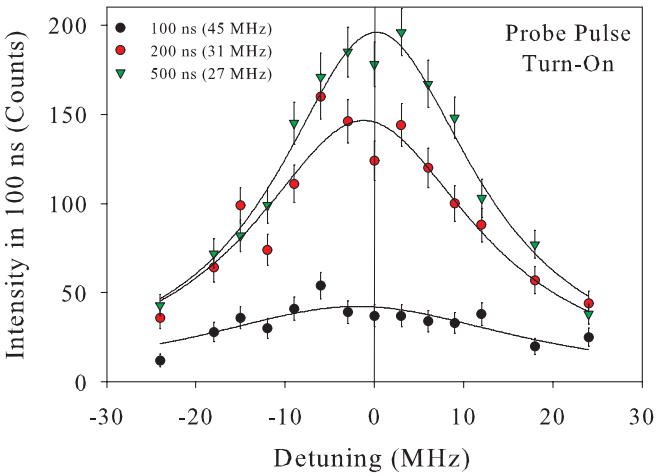

FIG. 9. (Color online) Time dependence of the spectral response of the atomic sample during the turn on of the weak-field probe excitation as a function of probe laser frequency detuning from bare atomic resonance. These data are recorded under conditions of the peak transverse optical depth $b_t = 165$.

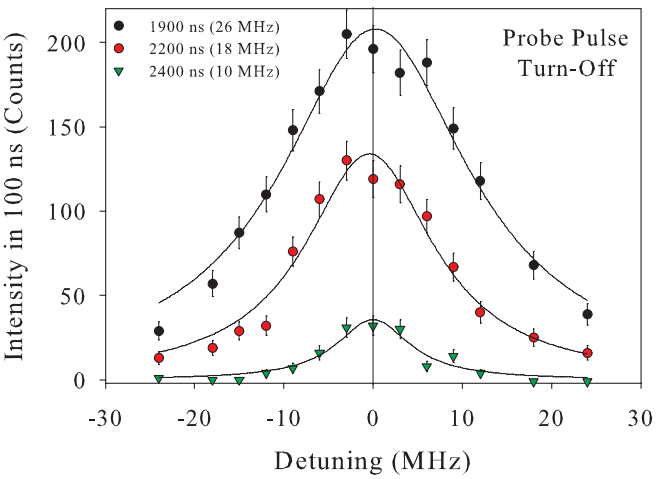

FIG. 11. (Color online) Time dependence of the spectral response of the atomic sample during the turn off of the weak-field probe excitation as a function of probe laser frequency detuning from atomic bare resonance. These data are recorded under conditions of the peak transverse optical depth $b_t = 165$.

-0.4 (4) MHz suggested by the data is of the right magnitude to correspond to the well-known Lorentz-Lorenz (local field) shift at these densities [69]. However, further measurements at higher density and with a spectrally narrower probe would be necessary to quantitatively examine the size of the shift.

3. *Time-dependent spectral response: Discussion*

We now turn to the excitation spectra for the full temporal range of the data; the experimental results are presented in Fig. 13. There we see the prompt narrowing, as mentioned before, of the spectral width of the excitation spectrum to a nearly steady level of around 20 MHz in about 500 ns. This approximately steady-state level persists until the probe is shut off, when there occurs a second fairly sharp decrease to a level just a bit larger than the 6 MHz natural linewidth of the resonance transition. Similar results are seen in the calculation of the full spectrum, as shown in Fig. 14. We note that the spectral width of the action spectra decreases slightly through most of the time period during which the probe pulse is on. We attribute this effect to the fact that for off-resonance excitation the effective optical depth is considerably less than for near-resonance excitation. This means that it takes longer for steady state in the scattered light intensity to be reached for near-resonance excitation. This behavior is also evident in Fig. 7, where the on-resonance intensity is increasing for the first microsecond or so of the signal. As the approach

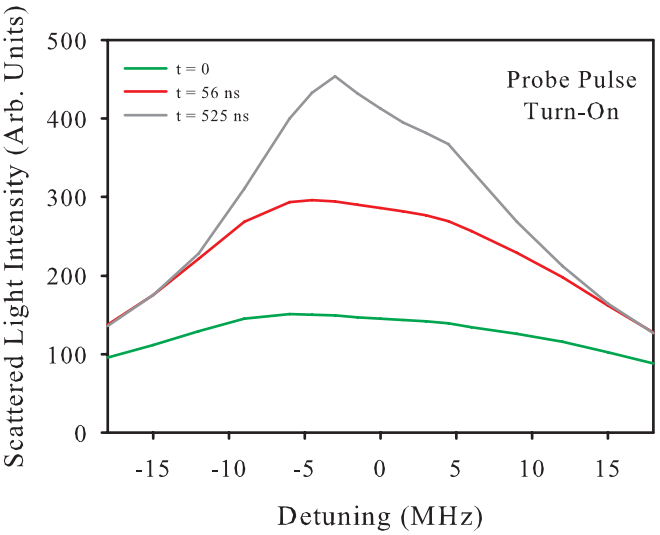

FIG. 10. (Color online) Calculated time dependence of the spectral response of the atomic sample during the turn on of the weak-field probe excitation as a function of probe laser frequency detuning from bare atomic resonance. These results are calculated for a peak density of $n_o = 0.05$.

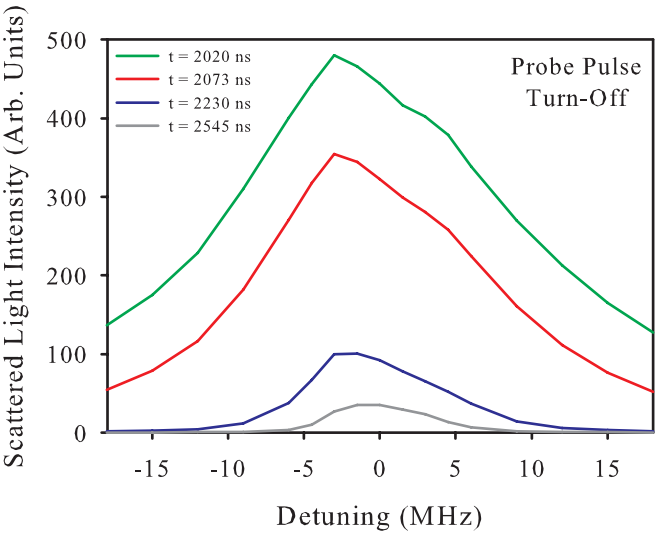

FIG. 12. (Color online) Calculated time dependence of the spectral response of the atomic sample during the turn off of the weak-field probe excitation as a function of probe laser frequency detuning from bare atomic resonance. These results are calculated for a peak density of $n_o = 0.05$.

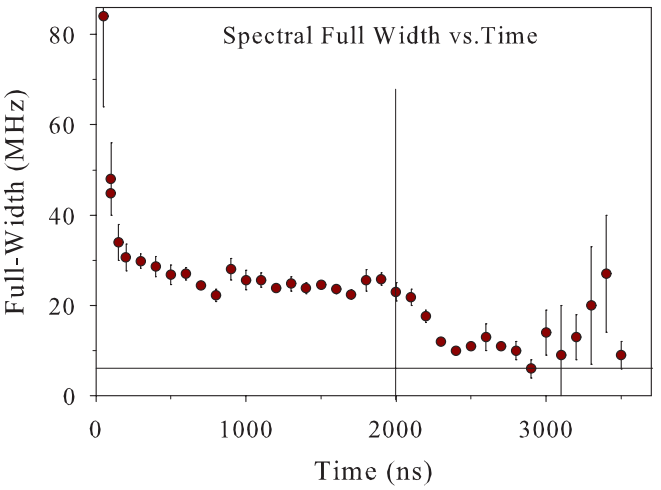

FIG. 13. (Color online) Time dependence of the spectral response of the atomic sample to weak-field probe excitation at different detunings from atomic bare resonance. These data are recorded under conditions of the peak transverse optical depth $b_t = 165$.

to steady state leads to an increased intensity near resonance, the effective full width at half maximum would be expected to decrease slightly, as it does.

We may gain some understanding of the experimental and theoretical results by recalling that the light scattering amplitudes may be determined by the poles of the projected resolvent matrix, as defined in the Appendix. In each realization of the atomic sample, for which the locations of the atoms are generally different, there is a set of poles, each consisting of a real and an imaginary part; these determine, respectively, the spectral location and the width of a resonance associated with a collective mode of excitation of the sample. For many realizations of the sample, a distribution of such collective states is found. Distributions for the real and imaginary parts of the poles are shown in Figs. 15 and 16. Plotted on the ordinate in each case is the number of states obtained normalized to

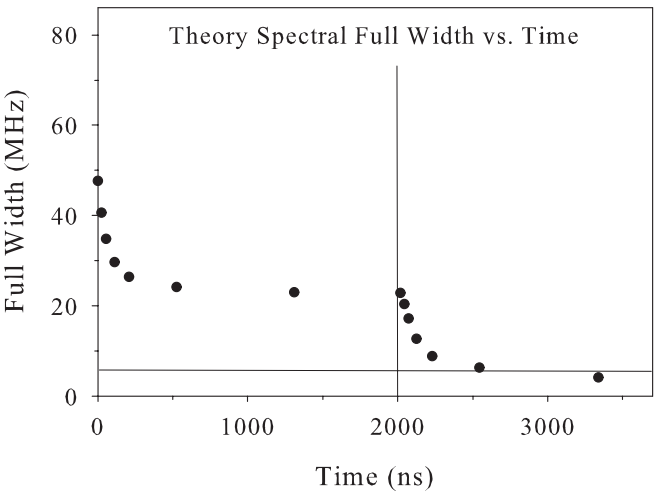

FIG. 14. Theoretical calculations of the time dependence of the spectral response of the atomic sample to weak-field probe excitation at different detunings from atomic bare resonance. These results are calculated for a peak density of $n_o = 0.05$.

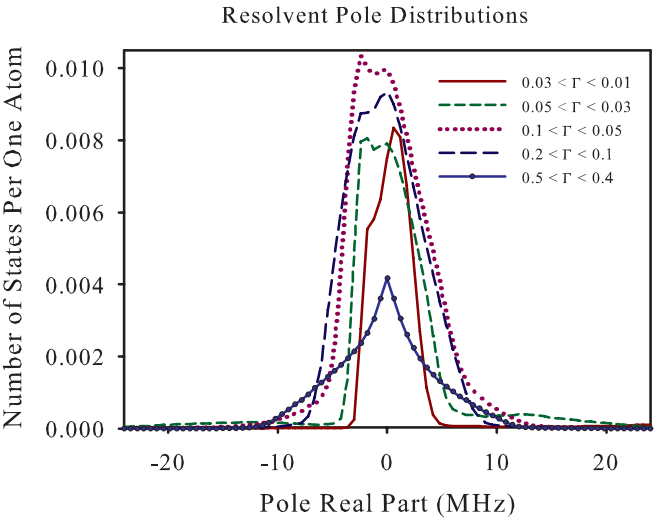

FIG. 15. (Color online) Distribution of the number of states per atom as a function of the real part of the pole of the resolvent. Results are shown accumulated within the indicated range of imaginary parts of the poles of the resolvent. The quantity Γ scales the relaxation rate associated with each pole according to $1/\Gamma = 26.24$ ns. These results are calculated for a peak density of $n_o = 0.05$.

the number of atoms. We note that dividing this quantity by the energy bin size in each case would result in a density of states. For the real parts of the poles (Fig. 14) this quantity is $0.1\gamma = 600$ kHz. For the imaginary parts of the poles (Fig. 16), the scale is $0.0025\gamma = 15$ kHz. Note also that the number of states for the real parts of the poles are grouped according to a range of decay rates, as indicated in the legend of Fig. 15. Similarly, in the legend of Fig. 16 the grouping of the number

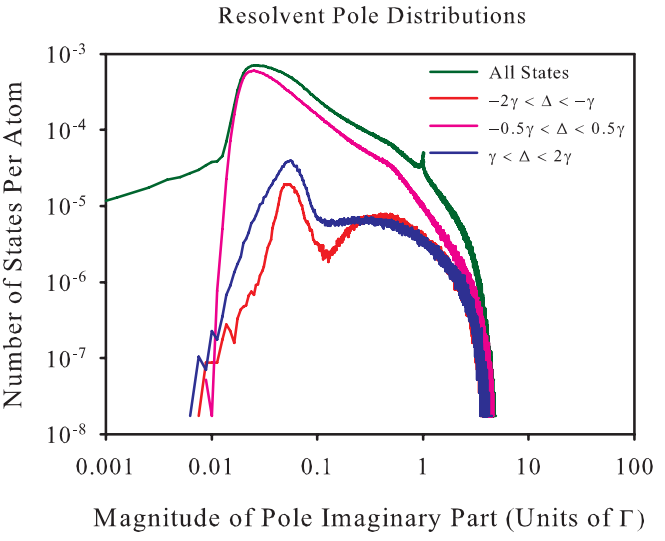

FIG. 16. (Color online) Distribution of the number of states per atom as a function of the imaginary part of the pole of the resolvent. Results are shown accumulated within the indicated range of imaginary parts of the poles of the resolvent. Note that all pole imaginary parts are negative; the magnitudes are plotted here. The quantity γ scales the detuning range associated with each pole according to $\gamma = 6$ MHz. These results are calculated for a peak density of $n_o = 0.05$.

of states for the imaginary parts of the poles is given in terms of different detuning ranges. This grouping allows us to obtain qualitative insights into the experimental behavior seen in Figs. 7, 9, 11, and 13, and the theoretical results of Figs. 8, 10, 12, and 14.

In considering the results of Fig. 13, we first reiterate that the initial response of the system consists of collective scattering from the atomic sample as a whole. This signal constitutes a very small part of the total scattered intensity at any time, and is observable only during the probe pulse turn-on period, a time interval on the order of the 50 ns scattering time [68]; see Fig. 7. It is spectrally broad and weak because the signals arise from a surface layer of about one absorption length in thickness and thus only a relatively small number of the atoms in the sample contribute. Multiple scattering becomes increasingly important at longer times, and steady state closely reached after a few hundred nanoseconds. Here the probe laser excites a distribution of quasimodes [44] having a characteristic resonance frequency and decay rate which correspond to the real and imaginary parts of the resolvent poles. In the steady-state mode excitation is balanced by mode decay and the nearly constant spectral width of the excitation spectrum reflects this. Once the probe laser is extinguished, the width of the excitation spectrum rapidly decreases. This is a reflection of the mode distribution having different lifetimes, as seen in Fig. 15. There the distribution of states is binned according to different decay rate bands, as defined in the legend. We see that the distribution of pole real parts indeed narrows as the modes of larger Γ die away.

We point out that the results in Fig. 15 allow us to make direct qualitative conclusions about the behavior of the optical response of dense clouds after the probe laser is switched off. However, the knowledge of the pole distribution is indispensable for accurate calculation of the dynamics of the system under study through all stages of its time evolution. In addition to the subradiant states analyzed in Fig. 15, in the steady-state regime, as well as during switching on of the probe, the super-radiant collective states also play an important role. In these stages it is very important to describe correctly the excitation of different collective states of the multiatom system by the external radiation. We emphasize that all these circumstances are taken into account in the general theory reviewed in the Appendix. Finally, let us reiterate that the calculations shown in Fig. 15 describe only the subradiant mode distribution, although the super-radiant distribution is quite similar. This is important for other aspects of the spectral response, because the overall width is determined by both the spectral position and lifetime (width) of all states (sub- and super-radiant) and by the nature of their excitation by the external field. In our case, as shown in an earlier report [61] the geometry of observation also plays an important role. In that paper we show that, for dense media, scattering in different directions has different spectral dependences.

Last, we turn to the longest-time decay evident in Fig. 7 as the longer tails appearing after the probe pulse has been turned off and the shorter-lived transients have died away. These transients have an associated lifetime of about 650(50) ns, and are independent of detuning over the range ± 6 MHz (reliable results could not be obtained for larger detunings). This is expected, as the longest-lived mode in the sample, the so-called Holstein mode, has a characteristic lifetime, but it is excited with lower efficiency at larger detunings. Inspection of the calculations in Fig. 15 shows the distribution of pole imaginary parts for different detuning bands. The graphs show that for detunings Δ larger than ± 6 MHz ($\pm\gamma$), the longest-lived modes (smallest Γ) are indeed suppressed. The longest-lived mode here implies a statistical value, because each realization of the atomic sample has a different spatial distribution of atoms. In Fig. 16, this is the peak of the "all states" distribution, and shows that for this particular average atom distribution the peak corresponds to a decay rate of about 0.025γ, and an associated lifetime of about 1 μs. Considering the physical differences between the model sample and the experimental one, as discussed earlier, this is in qualitative agreement with the experimental value of 650(50) ns.

IV. CONCLUSIONS

In this paper we have reported studies of near-resonance light scattering from dense and ultracold atomic rubidium. The density is sufficiently large that the experimental conditions are close to satisfying the Ioffe-Regel criterion for light localization on the optically closed $F = 2 \rightarrow F' = 3$ transition. We have observed collective effects associated with the density and detuning dependence, and suggestion of the influence of the dipole-dipole interaction between the Rb atoms. We have also observed evolution of the excitation spectral distributions towards spectrally narrow features indicative of long-lived modes within the sample. Results are also presented of theoretical treatments of the quantities determined in the experiments; very good correspondence between the experimental and theoretical results is obtained. Although the experimental results show collective effects, there was no evidence of cooperative effects, or clear evidence of very long-lived states which might be associated with Anderson localization of light in three dimensions. The experimental results are then understood, by comparison with theoretical calculations, in terms of multiple scattering at low temperatures where the effect of atomic velocity is minimal, and the time scales for effects associated with atomic recoil have not been attained. We conclude that, for the $F = 2 \rightarrow F' = 3$ transition, the large optical depth of the sample does not permit efficient injection of optical excitation to the highest-density central portion of the sample. Observation of localization effects then seems difficult using this scheme. One alternative is to use light shifts to manipulate the optical depth to achieve optical control of light injection into the samples; such exploration is now under way.

ACKNOWLEDGMENTS

We appreciate the financial support of the National Science Foundation (Grants No. NSF-PHY-0654226 and No. NSF-PHY-1068159) and the Russian Foundation for Basic Research (Grant No. RFBR-CNRS 12-02-91056). D.V.K. would like to acknowledge support from the External Fellowship Program of the Russian Quantum Center (Ref. No. 86). We also acknowledge the generous support of the Federal Program for Scientific and Scientific-Pedagogical Personnel of Innovative Russia (Contract No. 14.B37.21.1938).

APPENDIX: THEORETICAL APPROACH

In this section we provide a sketch of the approach we have used for the theoretical results presented in this paper. In this sketch, we follow the descriptions in our earlier papers [43,61] We consider the temporal dynamics of a system consisting of $N+1$ motionless atoms. N atoms form the cloud. These atoms are identical and have a ground state of angular momentum $J=0$ separated by the energy $\hbar\omega_a$ from an excited $J=1$ state. The decay constant of this state is taken as γ. One atom plays the role of the light source. It is located far from the cloud and has the same $J=0 \leftrightarrow J=1$ structure of levels but a different transition frequency ω_s and a different decay constant γ_s. We assume that initially all atoms of the cloud are in the ground state and the spatially separated source atom is in a coherent state which is a superposition of the ground and a small admixture of the excited state.

The system dynamics can be described by a nonstationary Schrödinger equation for the wave function ψ of the joint system consisting of atoms and the field generated in the process of the evolution:

$$i\hbar\frac{\partial\psi}{\partial t}=H\psi. \tag{A1}$$

The atom-field interaction is described in the dipole approximation:

$$V=-\sum_a \mathbf{d}^{(a)}\cdot\mathbf{E}(\mathbf{r}_a), \tag{A2}$$

$$\begin{aligned}\mathbf{E}(\mathbf{r})&=\mathbf{E}^{(+)}(\mathbf{r})+\mathbf{E}^{(-)}(\mathbf{r})\\&=i\sum_{\mathbf{k},\alpha}\sqrt{\frac{2\pi\hbar\omega_k}{\mathcal{V}}}\mathbf{e}_{\mathbf{k}\alpha}a_{\mathbf{k}\alpha}\exp(i\mathbf{k}\cdot\mathbf{r})+\text{H.c.},\end{aligned} \tag{A3}$$

where $\mathbf{E}^{(\pm)}$ are the operators of the positive and negative frequency components of the field; $a_{\mathbf{k}\alpha}$ is the photon annihilation operator in a mode with wave vector $\mathbf{k}$ and polarization α; $\mathcal{V}$ is the quantization volume; $\mathbf{d}^{(a)}$ is the dipole moment operator of the atom a; and $\mathbf{e}_{\mathbf{k}\alpha}$ are polarization unit vectors.

We look for a solution of the Schrödinger equation as a superposition of eigenstates of the operator H_0,

$$\begin{aligned}\psi=&\sum_{\mathbf{k}\alpha}b_{\mathbf{k}\alpha}(t)|g,g,\ldots,g\rangle\otimes|\mathbf{k}\alpha\rangle\\&+\sum_j b_j(t)|g,g,\ldots,g,e_j,g,\ldots,g\rangle\otimes|\text{vac}\rangle\\&+b'_0(t)|g,g,\ldots,g\rangle\otimes|\text{vac}\rangle\\&+\sum_{\mathbf{k}\alpha,j,l}b_{\mathbf{k}\alpha,j,l}(t)|g,\ldots,g,e_j,g,\ldots,g,e_l,g,\ldots,g\rangle\otimes|\mathbf{k}\alpha\rangle.\end{aligned} \tag{A4}$$

In the rotating-wave approximation it is enough to take into account only the two first items of this expression. States without excitation in either the atomic or the field subsystem allow us to describe coherent states of the source atom. Nonresonant states with two excited atoms and one photon are necessary for a correct description of the dipole-dipole interaction at short interatomic distances. Note that, in the considered case, there are three excited states for each atom $e=|J,m\rangle$, which differ by the value of angular momentum projection $m=-1,0,1$.

As an initial condition for Eq. (A1) we will consider the case when at $t=0$ the field is in a vacuum state, all atoms of the cloud are in the ground state, and the source atom, which we denote by the index s, is in a superposition of the ground and one of the excited states $|J,m\rangle$. Designating the corresponding amplitudes as b'_0 and b_0, we can write

$$\psi(0)=(b'_0|g,g,\ldots,g\rangle+b_0|e_{s0},g,g,\ldots,g\rangle)\otimes|\text{vac}\rangle, \tag{A5}$$

where the index e_{s0} corresponds to the one of the three possible states of atom s which is populated in the initial moment of time.

In the framework of the assumptions made, the amplitude $b'_0(t)$ does not change during the evolution of the system $b'_0(t)=b'_0$, because transitions between this and the other states taken into account are impossible.

To determine all other amplitudes we solve the set of equations which follows from (A1). We exclude amplitudes of states with one photon and obtain a finite closed system of equations for $b_e(t)\equiv b_{e_j}(t)$; $j\neq s$. For Fourier components $b_e(\omega)$ we have (at greater length see [61])

$$\sum_{e'\neq s}[(\omega-\omega_a)\delta_{ee'}-\Sigma_{ee'}(\omega)]\,b_{e'}(\omega)=\Lambda_{es}(\omega). \tag{A6}$$

The matrix elements $\Sigma_{ee'}(\omega)$ for e and e' corresponding to different atoms describe excitation exchange between these atoms. Assuming that in states $\psi_{e'}$ and ψ_e atoms b and a are excited, respectively, in the framework of the pole approximation, we have

$$\begin{aligned}\Sigma_{ee'}(\omega)=&\sum_{\mu,\nu}\frac{\mathbf{d}^{\mu}_{e_a;g_a}\cdot\mathbf{d}^{\nu}_{g_b;e_b}}{\hbar r^3}\\&\times\left\{\delta_{\mu\nu}\left[1-i\frac{\omega_a r}{c}-\left(\frac{\omega_a r}{c}\right)^2\right]\exp\left(i\frac{\omega_a r}{c}\right)\right.\\&\left.-\frac{\mathbf{r}_\mu\cdot\mathbf{r}_\nu}{r^2}\left[3-3i\frac{\omega_a r}{c}-\left(\frac{\omega_a r}{c}\right)^2\right]\exp\left(i\frac{\omega_a r}{c}\right)\right\}.\end{aligned} \tag{A7}$$

Here $\mathbf{r}_\mu$ is the projection of the vector $\mathbf{r}=\mathbf{r}_a-\mathbf{r}_b$ on the axis of the chosen coordinate system and $r=|\mathbf{r}|$ is the separation between atoms a and b.

If e and e' correspond to excited states of one atom then $\Sigma_{ee'}(\omega)$ differs from zero only for $e=e'$ ($m=m'$). In this case $\Sigma_{ee}(\omega)$ determines the Lamb shift and the decay constant of the corresponding excited state. Including Lamb shifts in the transition frequency ω_a we get

$$\Sigma_{ee}(\omega)=-i\gamma_a/2. \tag{A8}$$

The term $\Lambda_{es}(\omega)$ in the right-hand side of Eq. (A6) describes excitation of the cloud atoms by the radiation of the source. For modeling the time evolution of cloud excitation in a real experiment we assume that the decay constant of the source atom is very small, $\gamma_s\to 0$, and at the same time we employ the presence of a special shutter between the light source and the cloud. This allows us to simulate the effect of the shape of the experimental probe pulse, which is normally well characterized in experiments. The time profile

of the shutter $F(t)$ is taken as trapezoid. Neglecting the secondary excitation of the source atom s by reradiation from the cloud and assuming that the size of the atomic ensemble is negligible compared with the distance from it to the source, we have

$$\Lambda_{es}(\omega) = b_0 F(\omega)\widetilde{\Sigma}_{es}(\omega), \tag{A9}$$

$$\widetilde{\Sigma}_{es}(\omega) = -\sum_{\mu,\nu} \frac{k^2 \mathbf{d}^{\mu}_{e;g} \cdot \mathbf{d}^{\nu}_{g_s;e_s}}{\hbar r_s} \left[\delta_{\mu\nu} - \frac{\mathbf{k}_\mu \cdot \mathbf{k}_\nu}{k^2}\right] \times \exp\left(ikr_s + i\mathbf{k}\cdot\mathbf{r}_e\right). \tag{A10}$$

Here $\mathbf{k} = \omega\mathbf{n}/c$; $\mathbf{r}_e$ are radii locating the atoms; $\mathbf{n}$ is a unit vector oriented from the source to the cloud; and $F(\omega)$ is a Fourier transform of the excitation time profile $F(t)$.

Knowledge of explicit expressions for $\Lambda_{es}(\omega)$ and $\Sigma_{ee'}(\omega)$ allows us to determine the amplitudes of all onefold excited states.

Introducing the inverse matrix which, as shown in [43], is a resolvent operator of the considered system projected on the states consisting of the single-atom excitation, distributed over the ensemble, and the vacuum state for all the field modes,

$$R_{ee'}(\omega) = \left[(\omega - \omega_a)\delta_{ee'} - \Sigma_{ee'}(\omega)\right]^{-1}, \tag{A11}$$

we can write the solution of the system (A6) as follows:

$$b_e(\omega) = \sum_{e'\neq s} R_{ee'}(\omega)\Lambda_{e's}(\omega). \tag{A12}$$

For the amplitude $b_e(t)$ we get

$$b_e(t) = \int_{-\infty}^{\infty} \frac{d\omega}{2\pi} b_0 \exp(-i\omega t)F(\omega) \sum_{e'\neq s} R_{ee'}(\omega)\tilde{\Sigma}_{e's}(\omega). \tag{A13}$$

This relation gives the distribution of excited states at any instant of time. Knowing the amplitudes $b_e(t)$ allows us to determine all other amplitudes $b(t)$ coming into Eq. (A4) and consequently to calculate the properties of scattered light (for details see [61]), particularly the angular distribution, polarization, and time evolution of its intensity.

In the present work, to determine the time dynamics of the system we calculate the integral like (A13) by means of the residue theory. The poles of the matrix of the projected resolvent $R_{ee'}$ play a key role in the calculation. These poles are determined in turn by eigenstates of the matrix $\Sigma_{ee'}$. Decomposing the vector $\tilde{\Sigma}_{e's}$ over the eigenvector of the matrix $\Sigma_{ee'}$ we present the integral (A13) as the sum of separate pole contributions. The energy and decay constant of each pole depend on both the real and imaginary parts of the eigenvalues of $\Sigma_{ee'}$.

[1] H. J. Metcalf and P. van der Straten, *Laser Cooling and Trapping* (Springer, New York, 1999).

[2] R. Grimm, M. Weidemuller, and Y. Ovchinnokov, Adv. At. Mol. Opt. Phys. **42**, 95 (2000).

[3] C. J. Pethick and H. Smith, *Bose-Einstein Condensation in Dilute Gases* (Cambridge University Press, Cambridge, UK, 2002).

[4] S. Giorgini, L. P. Pitaevskii, and S. Stringari, Rev. Mod. Phys. **80**, 1215 (2008).

[5] Lev Pitaevskii and Sandros Stringari, *Bose-Einstein Condensation*, International Series of Monographs on Physics No. 113 (Oxford University Press, New York, 2003).

[6] Dirk Bouwmeester, Artur Ekert, and Anton Zeilinger, *The Physics of Quantum Information* (Springer-Verlag, Berlin, 2001).

[7] M. D. Lukin, Rev. Mod. Phys. **75**, 457 (2003).

[8] P. W. Milonni, *Fast Light, Slow Light, and Left-handed Light* (Taylor and Francis, New York, 2005).

[9] M. Fleishhauer, A. Imamoglu, and J. P. Marangos, Rev. Mod. Phys. **77**, 633 (2005).

[10] Lene Vestergaard Hau, Nat. Photonics **2**, 451 (2008).

[11] D. A. Braje, V. Balic, G. Y. Yin, and S. E. Harris, Phys. Rev. A **68**, 041801 (2003).

[12] S. Ospelkaus, A. Peer, K.-K. Ni, J. J. Zirbel, B. Neyenhuis, S. Kotochigova, P. S. Julienne, J. Ye, and D. S. Jin, Nat. Phys. **4**, 622 (2008).

[13] G. K. Campbell, A. D. Ludlow, S. Blatt, J. W. Thomsen, M. J. Martin, M. H. de Miranda, T. Zelevinsky, M. M. Boyd, J. Ye, S. A. Diddams, T. P. Heavner, T. E. Parker, and S. R. Jefferts, Metrologia **45**, 539 (2008).

[14] Jun Ye, S. Blatt, M. M. Boyd, S. M. Foreman, E. R. Hudson, Tetsuya Ido, B. Lev, A. D. Ludlow, B. C. Sawyer, B. Stuhl, and T. Zelinsky, Int. J. Mod. Phys. D **16**, 2481 (2007).

[15] Steven Rolston, Physics **1**, 2 (2008).

[16] Thomas C. Killian, Science **316**, 705 (2007).

[17] New J. Phys. **11** (2009), special issue, focusing on recent advances and opportunities in ultracold molecular physics. See particularly Lincoln D. Carr and Jun Ye, New J. Phys. **11**, 055009 (2009).

[18] Matthias Weidemüller and Claus Zimmermann, *Interactions in Ultracold Gases* (Wiley-VCH, Darmstadt, 2003).

[19] M. Fleischhauer and M. D. Lukin, Phys. Rev. A **65**, 022314 (2002).

[20] Y. O. Dudin, S. D. Jenkins, R. Zhao, D. N. Matsukevich, A. Kuzmich, and T. A. B. Kennedy, Phys. Rev. Lett. **103**, 020505 (2009).

[21] Mark D. Havey, Contemp. Phys. **50**, 587 (2009).

[22] G. Labeyrie, Mod. Phys. Lett. B **22**, 73 (2008).

[23] E. Akkermans and G. Montambaux, *Mesoscopic Physics of Electrons and Photons* (Cambridge University Press, Cambridge, UK, 2007).

[24] D. V. Kupriyanov, I. M. Sokolov, C. I. Sukenik, and M. D. Havey, Laser Phys. Lett. **3**, 223 (2006).

[25] Mark D. Havey and Dmitriy V. Kupriyanov, Phys. Scr. **72**, C30 (2005).

[26] R. Kaiser and M. D. Havey, Opt. Photonics News **16**, 38 (2005).

[27] C. A. Müller, T. Jonckheere, C. Miniatura, and D. Delande, Phys. Rev. A **64**, 053804 (2001).

[28] A. F. Ioffe and A. R. Regel, in *Progress in Semiconductors*, edited by A. F. Gibson, F. A. Kroger, and R. E. Burgess, Vol. 4 (Heywood, London, 1960), p. 237.

[29] Y. Kuga and J. Ishimaru, J. Opt. Soc. Am. A **1**, 831 (1984).
[30] P. E. Wolf and G. Maret, Phys. Rev. Lett. **55**, 2696 (1985).
[31] G. Labeyrie, F. de Tomasi, J.-C. Bernard, C. A. Müller, C. A. Miniatura, and R. Kaiser, Phys. Rev. Lett. **83**, 5266 (1999).
[32] B. R. Mollow, Phys. Rev. **188**, 1969 (1969).
[33] G. Labeyrie, C. A. Müller, D. S. Wiersma, Ch. Miniatura, and R. Kaiser, J. Opt. B: Quantum Semiclass. Opt. **2**, 672 (2000).
[34] Y. Bidel, B. Klappauf, J. C. Bernard, D. Delande, G. Labeyrie, C. Miniatura, D. Wilkowski, and R. Kaiser, Phys. Rev. Lett. **88**, 203902 (2002).
[35] G. Labeyrie, D. Delande, R. Kaiser, and C. Miniatura, Phys. Rev. Lett. **97**, 013004 (2006).
[36] G. Labeyrie, C. Miniatura, C. A. Müller, O. Sigwarth, D. Delande, and R. Kaiser, Phys. Rev. Lett. **89**, 163901 (2002).
[37] T. Chanelière, D. Wilkowski, Y. Bidel, R. Kaiser, and Ch. Miniatura, Phys. Rev. E **70**, 036602 (2004).
[38] D. V. Kupriyanov, I. M. Sokolov, and M. D. Havey, Opt. Commun. **243**, 165 (2004).
[39] P. Kulatunga, C. I. Sukenik, S. Balik, M. D. Havey, D. V. Kupriyanov, and I. M. Sokolov, Phys. Rev. A **68**, 033816 (2003).
[40] D. V. Kupriyanov, I. M. Sokolov, N. V. Larionov, P. Kulatunga, C. I. Sukenik, S. Balik, and M. D. Havey, Phys. Rev. A **69**, 033801 (2004).
[41] S. Balik, P. Kulatunga, C. I. Sukenik, M. D. Havey, D. V. Kupriyanov, and I. M. Sokolov, J. Mod. Opt. **52**, 2269 (2005).
[42] C. Cohen-Tannoudji, J. Dupont-Roc, and G. Grynberg, *Atom-Photon Interactions. Basic Processes and Applications* (John Wiley & Sons, New York, 1992).
[43] I. M. Sokolov, M. D. Kupriyanova, D. V. Kupriyanov, and M. D. Havey, Phys. Rev. A **79**, 053405 (2009).
[44] T. Bienaimé, R. Bachelard, N. Piovella, and R. Kaiser, Fortschr. Phys. **61**, 377 (2013).
[45] E. Akkermans, A. Gero, and R. Kaiser, Phys. Rev. Lett. **101**, 103602 (2008).
[46] T. Bienaime, S. Bux, E. Lucioni, Ph. W. Courteille, N. Piovella, and R. Kaiser, Phys. Rev. Lett. **104**, 183602 (2010).
[47] R. Bachelard, Ph. Courteille, R. Kaiser, and N. Piovella, Europhys. Lett. **97**, 14004 (2012).
[48] T. Bienaime, M. Petruzzo, D. Bigerni, N. Piovella, and R. Kaiser, J. Mod. Opt. **58**, 1942 (2011).
[49] H. Bender, C. Stehle, S. Slama, R. Kaiser, N. Piovella, C. Zimmermann, and Ph. W. Courteille, Phys. Rev. A **82**, 011404(R) (2010).
[50] S. Bux, E. Lucioni, H. Bender, T. Bienaime, K. Lauber, C. Stehle, C. Zimmermann, S. Slama, Ph. W. Courteille, N. Piovella, and R. Kaiser, J. Mod. Opt. **57**, 1841 (2010).
[51] P. W. Anderson, Phys. Rev. **109**, 1492 (1958).
[52] D. S. Wiersma, P. Bartolini, Ad Lagendijk, and R. Righini, Nature (London) **390**, 671 (1997).
[53] A. A. Chabanov, M. Stoytchev, and A. Z. Genack, Nature (London) **404**, 850 (2000).
[54] M. Storzer, P. Gross, C. M. Aegerter, and G. Maret, Phys. Rev. Lett. **96**, 063904 (2006).
[55] C. M. Aegerter and G. Maret, Prog. Opt. **52**, 1 (2009).
[56] Hui Cao, Prog. Opt. **45**, 510 (2003).
[57] D. S. Wiersma, Nat. Phys. **4**, 359 (2008).
[58] C. Conti and A. Fratalocchi, Nat. Phys. **4**, 794 (2008).
[59] L. S. Froufe-Pèrez, W. Guerin, R. Carminati, and R. Kaiser, Phys. Rev. Lett. **102**, 173903 (2009).
[60] W. Guerin, N. Mercadier, D. Brivio, and R. Kaiser, Opt. Express **17**, 11236 (2009).
[61] I. M. Sokolov, D. V. Kupriyanov, and M. D. Havey, J. Exp. Theor. Phys. **112**, 246 (2011).
[62] S. Balik, A. L. Win, and M. D. Havey, Phys. Rev. A **80**, 023404 (2009).
[63] For an ellipsoidal Gaussian atom distribution of sizes r_o and z_o and peak density n_o, $n(r) = n_o e^{-r^2/2r_o^2 - z^2/2z_o^2}$. The total number of atoms is $N = (2\pi)^{3/2} n_o r_o^2 z_o$ and the peak transverse (longitudinal) optical depth is $b_t = \sqrt{2\pi} n_o \sigma_o r_o$ ($b_l = \sqrt{2\pi} n_o \sigma_o z_o$). σ_o is the weak-field resonance light scattering cross section. The peak total cross section is given by $\frac{2F'+1}{2F+1}\frac{\lambda^2}{2\pi}$.
[64] I. M. Sokolov, A. S. Kuraptsev, D. V. Kupriyanov, M. D. Havey, and S. Balik, J. Mod. Opt. **60**, 50 (2013).
[65] Reprinted with permission from the publisher (Taylor & Francis Ltd, http://www.tandf.co.uk/journals), from Ref. [64].
[66] A. S. Kuraptsev, I. M. Sokolov, and Ya. A. Fofanov, Opt. Spectrosc. **112**, 401 (2012).
[67] Ya. A. Fofanov, A. S. Kuraptsev, I. M. Sokolov, and M. D. Havey, Phys. Rev. A **84**, 053811 (2011).
[68] E. P. Wigner, Phys. Rev. **98**, 145 (1955).
[69] J. J. Maki, M. S. Malcuit, J. E. Sipe, and R. W. Boyd, Phys. Rev. Lett. **67**, 972 (1991).